Draft version April 8, 2014
Preprint typeset using LaTeX style emulateapj v. 04/17/13

FINGERPRINTS OF GALACTIC LOOP I ON THE COSMIC MICROWAVE BACKGROUND

Hao Liu
Niels Bohr Institute and DISCOVERY Center, Copenhagen University, Blegdamsvej 17, 2100 Copenhagen Ø, Denmark and
Institute of High Energy Physics, CAS, Beijing, China

Philipp Mertsch
Kavli Institute for Particle Astrophysics & Cosmology, 2575 Sand Hill Road, M/S 29, Menlo Park, CA 94025, USA

Subir Sarkar
Rudolf Peierls Centre for Theoretical Physics, University of Oxford, 1 Keble Road, Oxford OX1 3NP, UK and
Niels Bohr International Academy, Copenhagen University, Blegdamsvej 17, 2100 Copenhagen Ø, Denmark

Draft version April 8, 2014

ABSTRACT

We investigate possible imprints of galactic foreground structures such as the 'radio loops' in the derived maps of the cosmic microwave background. Surprisingly there is evidence for these not only at radio frequencies through their synchrotron radiation, but also at microwave frequencies where emission by dust dominates. This suggests the mechanism is magnetic dipole radiation from dust grains enriched by metallic iron, or ferrimagnetic molecules. This new foreground we have identified is present at high galactic latitudes, and potentially dominates over the expected B-mode polarisation signal due to primordial gravitational waves from inflation.

1. INTRODUCTION

The study of the cosmic microwave background (CMB) radiation is a key testing ground for cosmology and fundamental physics, wherein theoretical predictions can be confronted with observations (Larson et al. 2011; Ade et al. 2013a,b). The temperature fluctuations in the CMB have provided our deepest probe of the Big Bang model and of the nature of space–time itself. Moreover CMB data provide a bridge between cosmology and astro-particle physics, shedding light on galactic cosmic rays (Mertsch & Sarkar 2013), and galactic X- and γ-ray emission (Aghanim et al. 2011a,b; Ade et al. 2012).

Ever since the first release of data from the *Wilkinson Microwave Anisotropy Probe* (WMAP), it has been noted that the derived CMB sky maps exhibit departures from statistical isotropy (Chiang et al. 2003, 2008; de Oliveira-Costa et al. 2004; Copi et al. 2004; Schwarz et al. 2004; Park 2004; Eriksen et al. 2004; Land & Magueijo 2005, 2007; Copi et al. 2007; Cruz et al. 2008; Hoftuft et al. 2009; Hansen et al. 2009; Kim & Naselsky 2010), probably because of residuals from the incomplete removal of galactic foreground emission. For example the Kuiper Belt in the outer Solar System may partly be responsible for the unexpected quadrupole-octupole alignment and parity asymmetry in the CMB (Hansen et al. 2012a) This issue has acquired even more importance after the first release of cosmological data products from the *Planck* satellite (Ade et al. 2013c).

In this paper we construct a physical model to account for the local features of the WMAP internal linear combination (ILC) map (Bennett et al. 2013) in the direction of the galactic 'radio loops', in particular Loop I (Berkhuijsen et al. 1971). We show that in the low multipole domain, $\ell \leq 20$, the peaks of the CMB map correlate with radio synchrotron emission from Loop I. However, the physical source of this anomaly is likely related to emission from dust — very probably magnetic dipole emission from dust grains enriched by metallic Fe, or ferrimagnetic molecules like Fe_3O_4 (Draine & Lazarian 1998, 1999).

Since supernova explosions will likely mix the dust grains and the magnetic field, it is quite plausible that magnetic dipole emission from dust and synchrotron emission from high energy electrons are both at work in Loop I, tracing the same signal morphology. The corresponding dust temperature anisotropy of Loop I can be as large as $20\,\mu$K, which is comparable to the amplitude of the CMB quadrupole. Moreover, part of the Loop I anomaly overlaps spatially with the *Planck* haze at 30 GHz (Ade et al. 2012). We are investigating these issues in more detail and will present the results elsewhere.

The structure of this paper is as follows: In Sec. 2 we summarize the properties of Loops I-IV from radio waves to X-rays. In Sec. 3 we demonstrate that there are spatial correlations between features in the WMAP 9-year ILC map and Loop I — the CMB temperature of the ILC map along Loop I is systematically shifted by $\sim 20\,\mu$K. We perform a cluster analysis along a ring defined by the radio emission from Loop I and show that the peaks of the CMB map are indeed clustered in this ring with a chance probability of about 10^{-4}. In Sec. 4, we discuss how this signal from Loop I could have evaded foreground subtraction using the ILC method. In Sec. 5 we discuss physical mechanisms of the emission from the Loop I region and argue that it likely arises from interstellar dust with a magnetic dipole moment. We present our conclusions in Sec. 6.

2. THE RADIO LOOPS IN THE MILKY WAY

Radio surveys of the Galaxy reveal a number of features that are parts of larger, so-called radio loops (Berkhuijsen et al. 1971). The most prominent is the North-Polar Spur (NPS) which is part of Loop I (Roger et al. 1999). It has been noted that the

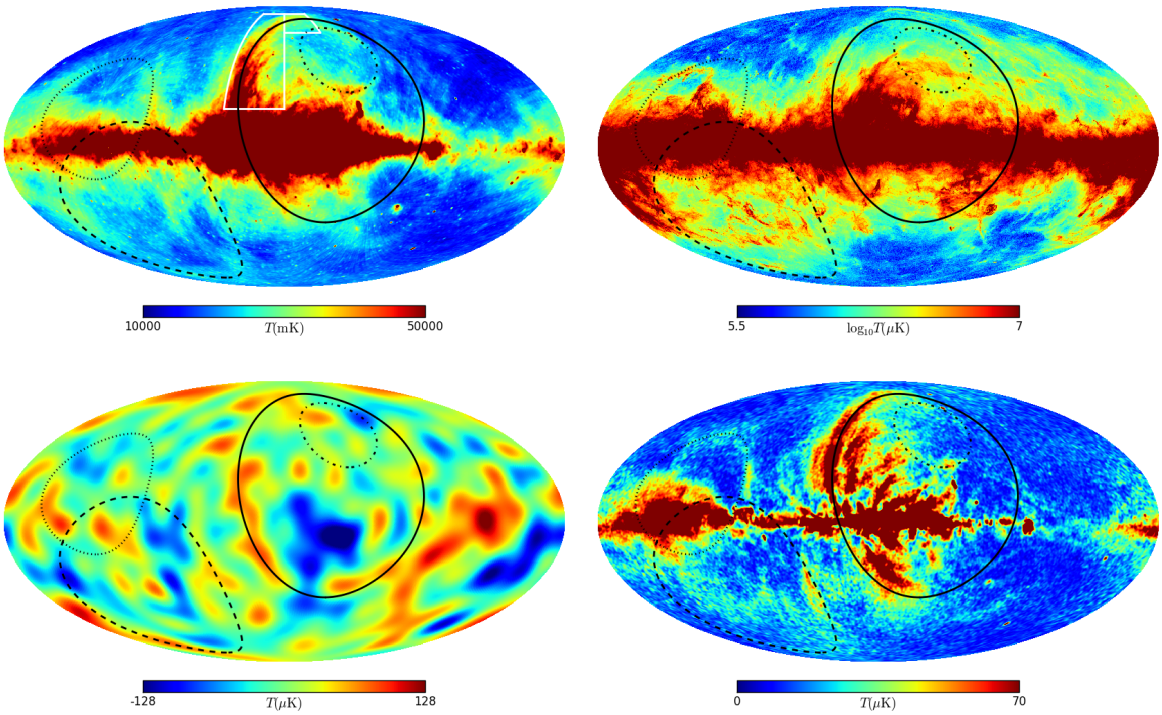

Figure 1. The 408 MHz survey (top left), the *Planck* 857 GHz map (top right) the low resolution ($l \leq 20$) WMAP9 ILC map (bottom left) and the WMAP9 K-band polarised intensity map (bottom right), with the positions of the radio loops indicated: Loops I-IV are indicated by the solid, dashed, dotted and dash-dotted line, respectively. The white outline (upper left panel) marks the NPS at 22 MHz.

radio loops correlate with expanding shells of gas and dust, energized by supernovae or stellar winds (Berkhuijsen et al. 1971; Heiles et al. 1980; Salter 1982; Wolleben 2007). The Loop I superbubble has been attributed to stellar winds from the Sco-Cen OB association and supernova activity, with the NPS being the brightest segment of a supernova remnant (SNR). The ambient magnetic field is most likely draped around the expanding bubbles (Heiles et al. 1980), as seen in radio and optical polarisation data. The NPS is observed over a wide range of wavelengths — the 21 cm IRAS survey, the ROSAT X-ray surveys at 0.25, 0.75 and 1.5 keV, and soft and hard γ-ray sky maps from EGRET and *Fermi*-LAT. It has also been detected in the WMAP K-band intensity and polarization maps, and more recently in the 2013 *Planck* 30 GHZ temperature map (Ade et al. 2013a), and even in the 353-857 GHz near-IR maps. Hansen et al. (2012b) have suggested from a cross-correlation of Faraday rotation and WMAP maps that such structures may affect the measured CMB temperature at high galactic latitudes.

Throughout this paper, we adopt the properties of Loops I-IV as given by Berkhuijsen et al. (1971) in their Tbl. 1. In Fig.1 we show the 408 MHz all-sky survey (Haslam et al. 1982), and 2013 *Planck* 857 GHz maps, indicating the positions of the four radio loops. For comparison, the loops are also shown superimposed on the low resolution ($\ell \leq 20$) WMAP9 ILC — hereafter called ILC9 — and K-band polarisation intensity maps.

3. CMB PEAKS ALONG LOOP I

To investigate possible correlations between the radio loops and features in the ILC9 map, we examine a ring of width $\pm 2^\circ$ along Loop I. The average temperature of the ILC9 signal along the $\pm 2^\circ$ ring, $\overline{T} = 1/(2\pi) \int_0^{2\pi} \mathrm{d}\Phi \, (T_{\rm ILC}(\Phi) - \overline{T}_{\rm ILC}) \simeq 23.9\,\mu$K, deviates significantly from the expectation for a random realisation of the CMB. In order to quantify this, we have generated 1000 CMB realizations of the 2013 WMAP best fit ΛCDM cosmological model (Bennett et al. 2013). Computing the number of simulated realisations with an average temperature equal or larger than the observed $\overline{T} = 23.9\,\mu$K, we find a p-value of only 0.01.

We have also determined the skewness of the distribution of ILC9 temperatures along the $\pm 2^\circ$ Loop I ring: $\gamma_1 = 1/(2\pi) \int_0^{2\pi} \mathrm{d}\Phi \, \left[(T_{\rm ILC}(\Phi) - \overline{T}_{\rm ILC}(\Phi))/\sigma\right]^3 \simeq -0.68$, where σ is the standard deviation of the ILC9 temperatures. Comparing this with the skewness of 1000 MC simulations we find a similarly small p-value of 0.03.

We interpret these anomalies as warranting a more detailed analysis. In order to show the result more clearly, we have investigated the statistical isotropy in a $\pm 10^\circ$ ring around Loop I, using a cluster analysis (Naselsky & Novikov 1995) that has been applied previously to WMAP data (Naselsky et al. 2004): If the ILC9 map is statistically isotropic, there should be no correlation between the position of its peaks and the position of Loop I. We therefore test the hypothesis that the distribution of the positive peaks around Loop I is *not* random.

As seen in Figs. 2, about 10 positive and 4 negative peaks of the ($\ell \leq 20$) ILC9 signal in the interval $[-88\,\mu\mathrm{K}, 88\,\mu\mathrm{K}]$ are clustered around Loop I. To quantify this, we compute for each pixel the angular distance G from Loop I along great circles crossing both the pixel and the loop center. Fig. 3 shows the average distance $\langle G \rangle$ for all pixels in a $\pm 10^\circ$ wide ring around Loop I, averaged in $\Delta T = 3\,\mu$K bins. It is apparent that on average,

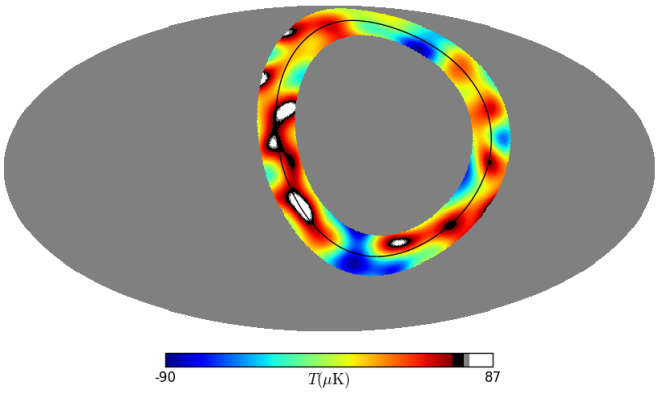

Figure 2. WMAP ILC temperature in a $\pm 10^\circ$ ring around Loop I. The white zones correspond to the four bins with the highest temperature, the grey zones show the effect of adding the next bin, and the black zones indicate the effect of adding two more bins.

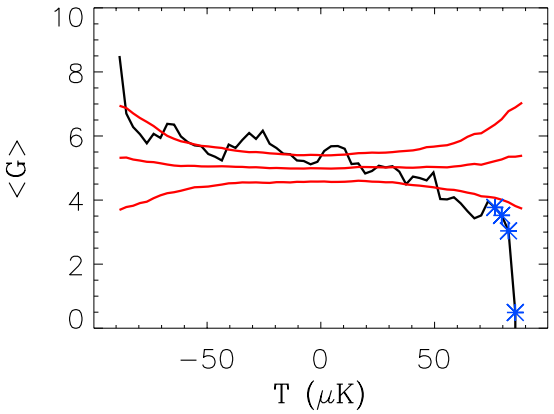

Figure 3. The average angular distance to Loop I versus temperature. The curve is descending, indicating that higher temperature pixels are closer to Loop I. The red lines show the $\pm 1\sigma$ range, while the 4 highest temperature bins are marked by asterisks.

pixels with higher temperature are closer to Loop I, i.e., the peaks in temperature are clustered along Loop I. To quantify the chance probability of this we have generated 100,000 CMB maps from the WMAP best fit ΛCDM cosmological model (Bennett et al. 2013). We determine the fraction of mock maps that have an average angular distance g_i smaller than the observed angular distance G_i in bin i. Only 18 of the 100,000 mock maps satisfy $g_i < G_i$ for all four last bins. In Tbl. 1, we list the probabilities for the clustering around Loop I to occur by chance, adopting different criteria. In the sky map in Fig. 2, the pixels in the four highest temperatures bins are marked white, while the pixels in the fifth (sixth and seventh) highest temperature bins are marked grey (black).

4. THE LOOP I ANOMALY AS A RESIDUAL FROM THE CMB FOREGROUNDS SEPARATION

We now turn to the question how a *physical* galactic emission could have evaded the foreground cleaning process. The ILC method for isolation of the CMB signal is based on the independence of its temperature on frequency. The temperature $S_j(\hat{\mathbf{n}})$ in frequency band j and direction $\hat{\mathbf{n}}$ is a superposition of the primordial CMB, $c(\hat{\mathbf{n}})$, and a sum $F_j(\hat{\mathbf{n}})$ of the galactic and extragalactic

Criterion	Probability
$g_i < G_i$ for all 4 bins	0.018%
$g_i < G_i$ for any 3 in 4 bins	2.0%
$g_i < G_i$ for any 2 in 4 bins	3.3%
$g_i < G_i$, $i = 1$ ($T = 85$ μK)	0.1%
$g_i < G_i$, $i = 2$ ($T = 82$ μK)	2.9%
$g_i < G_i$, $i = 3$ ($T = 79$ μK)	7.5%
$g_i < G_i$, $i = 4$ ($T = 76$ μK)	8.6%
$\sum_i g_i < \sum_i G_i$, $i = 1 \sim 4$	1.0%

Table 1
The probabilities for $g_i < G_i$ ($i = 1 \sim 4$) for the highest 4 bins under different criteria, evaluated with 100,000 MC simulations.

foregrounds, as well as instrumental noise:

$$S_j(\hat{\mathbf{n}}) = c(\hat{\mathbf{n}}) + F_j(\hat{\mathbf{n}})\,. \tag{1}$$

For regions of the sky outside the galactic mask, the estimator of the CMB anisotropy $d(\hat{\mathbf{n}})$ is given by an internal linear combination of the N different frequency bands:

$$d(\hat{\mathbf{n}}) = \sum_j W_j S_j(\hat{\mathbf{n}}) = c(\hat{\mathbf{n}}) + \sum_j W_j F_j(\hat{\mathbf{n}})\,. \tag{2}$$

The weights are chosen so as to preserve unit response to the CMB, i.e. $\sum_j W_j = 1$, and to minimise contamination by foregrounds. The reconstruction of the CMB $c(\hat{\mathbf{n}})$ through the estimator $d(\hat{\mathbf{n}})$ is exact, if and only if

$$\varepsilon(\hat{\mathbf{n}}) \equiv d(\hat{\mathbf{n}}) - c(\hat{\mathbf{n}}) = \sum_j W_j F_j(\hat{\mathbf{n}}) = 0. \tag{3}$$

Since the coefficients W_j are independent of $\hat{\mathbf{n}}$, eq. (3) presumes that the frequency dependence of the foregrounds is also *independent* of $\hat{\mathbf{n}}$. E.g. for a power law frequency dependence,

$$F_j(\hat{\mathbf{n}}) = F_0(\hat{\mathbf{n}}) \left(\frac{\nu_j}{\nu_0}\right)^{\alpha_j}\,, \tag{4}$$

the α_j are taken to be constants, i.e. the morphology of the foregrounds is assumed to be the same in all bands. Here, ν_j is the frequency of the j-th band, while $F_0(\hat{\mathbf{n}})$ is the foreground sky map at the reference frequency ν_0.

In practice this assumption cannot be fully valid, since the transition from the low frequency domain (e.g. the WMAP K band which is contaminated by synchrotron emission), to the high frequency domains (e.g. the WMAP W band which is contaminated by dust emission), leads to significant variability of the spectral index $\alpha_j(\hat{\mathbf{n}})$. Clearly no method for optimisation of the difference $d(\hat{\mathbf{n}}) - c(\hat{\mathbf{n}})$ can be free from the residuals of foregrounds for which $\varepsilon(\hat{\mathbf{n}}) \neq 0$. There is also an ultimate limit to the accuracy with which the CMB map can be reconstructed due to its chance correlations with the foregrounds. Consequently, some areas of the reconstructed CMB map may be contaminated by foreground residuals. An example is the contamination of the ILC map by residuals after removal of point sources, which produces non-Gaussian features in the derived CMB signal. We now show in a very general way, that a similar effect may be causing the anomaly in the Loop I region.

We start by considering a simple 'toy model'. Suppose that between frequencies $\nu_{\rm min}$ and $\nu_{\rm max}$ the area of Loop I is contaminated by an anomalous black body spectrum with temperature $T_s \sim 20\,{\rm K} \gg T_{\rm CMB}$ and optical depth

$\tau \sim 10^{-6}$, modifying eq. (1) to:

$$S_j(\hat{\mathbf{n}}) = c(\hat{\mathbf{n}}) + F_j(\hat{\mathbf{n}}) + \tau(\hat{\mathbf{n}}) T_s \Theta(\nu_{\rm min} \leq \nu_j \leq \nu_{\rm max}) \,. \quad (5)$$

Suppose further that the frequency interval $[\nu_{\rm min}, \nu_{\rm max}]$ affects a subset $\{j\} = \{1, \ldots N_c\}$ of the N frequency bands. The error function $\varepsilon(\hat{\mathbf{n}})$ is then

$$\varepsilon(\hat{\mathbf{n}}) = \sum_{j=1}^{N} W_j F_j(\hat{\mathbf{n}}) + \sum_{j=1}^{N_c} W_j \tau(\hat{\mathbf{n}}) T_s \,. \quad (6)$$

The second term, $\sum_{j=1}^{N_c} W_j \tau(\hat{\mathbf{n}}) T_s$, will make an anomalous contribution to the reconstructed CMB signal in the Loop I region. If this anomaly has the same frequency dependence as other foregrounds, the ILC method would have efficiently suppressed its contribution. Conversely, the existence of the observed anomaly (Sec. 3) implies that, at least locally (in this case in the direction of Loop I), its spectrum must be *different*.

We can estimate the spectrum of the anomalous emission by comparing the weight coefficients derived from the Loop I region, $W_j^{\rm Loop\ I}$, to those derived from the full sky excluding the Loop I region, $W_j^{\rm rest}$. To this end, we adopt a minimal variance approach (see Chiang et al. (2008); Bennett et al. (2013) for details). The weights for the WMAP K, Ka, Q, V, W bands are: $W_j^{\rm rest} = (-0.039, -0.384, 0.245, 0.991, 0.187)$ and $W_j^{\rm Loop\ I} = (-0.139, -0.286, 0.216, 0.457, 0.752)$, respectively. We note that since the fraction of the sky covered by Loop I is relatively small, the weight coefficients found for the sky (outside the mask) are very similar whether or not the Loop I region is included.

However, the weights for the Loop I region and for the rest of the sky, $W_j^{\rm Loop\ I}$ and $W_j^{\rm rest}$, are indeed different. In Fig. 4 we show the ILC maps obtained with each set of coefficients, and their difference. The difference map clearly indicates the presence of the Loops while showing little sign of the CMB. Furthermore, we can use the partial sums of above coefficients to estimate the frequency dependence of the anomaly: Whereas coefficients including the Q-band cancel efficiently, the series gets its largest contribution from the V-band, $\sum_{j=K}^{V}(W_j^{\rm rest} - W_j^{\rm Loop\ I}) = 0.565$. We note that while the $W_j^{\rm rest}$ decrease in the W-band, the $W_j^{\rm Loop\ I}$ continue to rise, suggesting that the anomalous emission extends beyond the W-band.

5. PHYSICAL MODELS OF THE PEAKS ALONG LOOP I

Adopting the synchrotron model for the radio loops (Sarkar 1983; Mertsch & Sarkar 2013) we have produced maps (with $l \leq 20$) for Loop I at the WMAP frequencies (22.8-93.5 GHz). With the $W_j^{\rm rest}$ from above, the ILC method suppresses $|T_{\rm synch}|$ from Loop I from $\sim 100\,\mu$K at 22.8 GHz to $\sim 10\,\mu$K in the ILC map, however with an effective *negative* weight. We conclude therefore that synchrotron emission cannot be responsible for the anomalies observed in the WMAP ILC map, and we should look instead at emission by the dust grains from the area of the Loop I.

The shells of old supernova remnants like Loop I are expected to strongly mix magnetic fields and interstellar gas and dust. This can explain how the CMB anomaly along Loop I which is spatially defined by its synchrotron radiation may in fact be due to emission from dust.

To further investigate the frequency dependence we have studied the correlation of the ILC temperature map $T_{\rm ILC}$ with the WMAP W- and V-band polarisation maps, $P_{\rm W}$ and $P_{\rm V}$. The latter have not entered into the production of the ILC map and are furthermore expected to be dominated by polarised dust. Therefore, their correlation with the ILC map gives us an *independent* handle on the contamination of the Loop I region by dust emission. We have computed the ratio of the polarised intensity in the W- and V-band, averaged over the $\pm 10^\circ$ wide ring (see Fig. 2) and find $\overline{P_{\rm W}/P_{\rm V}} = 1.7$ (which changes by less than 5% with a different ring width e.g. $\pm 2^\circ$). If the temperature anisotropy in this sample is weakly dependent on frequency ν, and $T(\nu) \simeq \overline{T} \simeq 23\,\mu$K (at least for the WMAP V and W bands) this value of 1.7 indicates the existence of *two* dust components in the Loop I region by the following argument.

Suppose that the anomalous emission is associated with a single thermal dust component. According to the *Planck* all-sky dust emission model (Abergel et al. 2013b,a), the temperature of the dust in units of the CMB thermodynamic temperature in the direction $\hat{\mathbf{n}}$ is:

$$T(\nu, \hat{\mathbf{n}}) = T(\nu_0, \hat{\mathbf{n}}) \frac{c(\nu)}{c(\nu_0)} \frac{e^{\frac{h\nu_0}{kT_{\rm d}(\mathbf{r})}} - 1}{e^{\frac{h\nu}{kT_{\rm d}(\hat{\mathbf{n}})}} - 1} \left(\frac{\nu}{\nu_0}\right)^{\beta(\hat{\mathbf{n}})+1} ,$$
$$c(\nu) = \left(2 \sinh \frac{x}{2} / x\right)^2 , \quad (7)$$

where $T_{\rm d}$ is the temperature of the dust, $x \equiv h\nu/kT_{\rm CMB} \approx \nu/56.8\,$GHz and ν_0 and $T(\nu_0, \hat{\mathbf{n}})$ are the reference frequency and temperature map, respectively. Now, adopting a dust temperature $T_{\rm d} = 20\,$K (see Abergel et al. (2013a)) and assuming that the polarisation fraction P/T is the same in the V- and W-bands, the spectral index β for dust emissivity should be unity. However, inspection of Fig. 9 of Abergel et al. (2013a) shows that the average spectral index for the Loop I region (see Fig. 2) is $\beta_{\rm pl} \simeq 1.6$. (This number is relatively robust as a different $\beta_{\rm pl}$ would lead to a vastly different extrapolated temperature.) Furthermore, our finding $\overline{P_{\rm W}/P_{\rm V}} = 1.7$ indicates that the temperature must be closely proportional to frequency, at least for the V and W bands i.e. in the range 61–94 GHz.

An alternative explanation of the anomalous emission from Loop I may be *magnetic* dipole emission from dust grains, arising from thermal fluctuations in the magnetisation of grain materials (Draine & Lazarian 1999; Draine & Hensley 2013). As mentioned above, this emission is required to extend beyond the W- and V-bands. It has been noted that this can be the case if the grain material is ferromagnetic (i.e. enriched with metallic Fe) or ferrimagnetic (e.g. magnetite, Fe_3O_4). Such grains may generate magnetic dipole emission extending up to 200–300 GHz and it has been argued that this accounts for the surprisingly strong sub-mm and mm emission from the Small Magellanic Cloud (Draine & Hensley 2012). This radiation may be particularly strong from the galactic loops too, reflecting the enrichment of interstellar matter by iron due to supernova explosions. If the temperature of the dust grains is around 18–20 K, a pop-

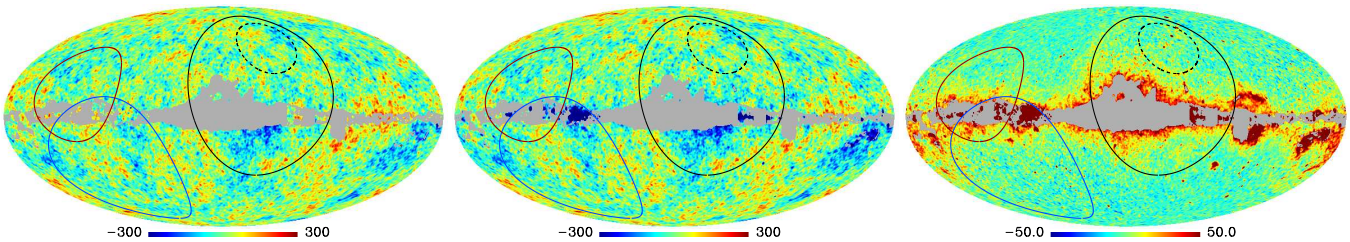

Figure 4. The ILC map generated using $W_j^{\rm rest}$ (left), $W_j^{\rm Loop\ I}$ (middle), and their difference (right), with the radio loops superimposed.

ulation of Fe grains or grains with Fe inclusions would be expected to produce strong emission near 70 GHz in the vicinity of the Fröhlich resonance for spherical dust grains. This peak would be broadened if the Fe grains or inclusions are not quite spherical, since the Fröhlich resonance frequency depends on the particle shape (see Fig.7 of Draine & Lazarian (1999)). At 120–130 GHz the magnetic dipole emission from dust grains will reach the limit of the thermal electric dipole 'vibrational' emission, while well above 200 GHz its contribution will be negligible relative to thermal emission from dust.

6. CONCLUSION

We have found evidence of local galactic structures such as Loop I in the ILC map of the CMB which is supposedly fully cleaned of foreground emissions. This contamination extends to high galactic latitude so the usual procedure of masking out the Milky Way cannot be fully effective at removing it. It extends to sufficiently high frequencies that it cannot be synchrotron radiation but is more likely magnetic dipole emission from ferro- or ferrimagnetic dust grains, as suggested by theoretical arguments (Draine & Lazarian 1999; Draine & Hensley 2013). This radiation is expected to be highly polarised.

It has not escaped our attention that the lower part of Loop I, in particular the additional loop structure identified by Wolleben (2007), crosses the very region of the sky from which the BICEP 2 experiment has recently detected a B-mode polarisation signal (Ade et al. 2014). This has been ascribed to primordial gravitational waves from inflation because "available foreground models" do not correlate with the BICEP maps. The new foreground we have identified is however *not* included in these models. Hence the cosmological significance if any of the detected B-mode signal needs further investigation. Forthcoming polarisation data from the *Planck* satellite will be crucial in this regard.

ACKNOWLEDGEMENTS

We are indebted to Bruce Draine, Pavel Naselsky and Andrew Strong for helpful discussions and to the Discovery Center for support. Hao Liu is supported by the National Natural Science Foundation of China (Grant No. 11033003 & 11203024), and the Youth Innovation Promotion Association, CAS. Philipp Mertsch is supported by DoE contract DE-AC02-76SF00515 and a KIPAC Kavli Fellowship. Subir Sarkar acknowledges a DNRF Niels Bohr Professorship.

REFERENCES

Abergel, A., et al. 2013a, arXiv:1312.1300
—. 2013b, arXiv:1312.5446
Ade, P., et al. 2012, arXiv:1208.5483
—. 2013a, arXiv:1303.5075
—. 2013b, arXiv:1303.5076
—. 2013c, arXiv:1303.5083
—. 2014, arXiv:1403.3985
Aghanim, N., et al. 2011a, arXiv:1106.1376
—. 2011b, arXiv:1112.5595
Bennett, C., et al. 2013, Astrophys.J.Suppl., 208, 20
Berkhuijsen, E. M., Haslam, C. G. T., & Salter, C. J. 1971, A&A, 14, 252
Chiang, L.-Y., Naselsky, P. D., & Coles, P. 2008, Mod.Phys.Lett., A23, 1489
Chiang, L.-Y., Naselsky, P. D., Verkhodanov, O. V., & Way, M. J. 2003, Astrophys.J., 590, L65
Copi, C., Huterer, D., Schwarz, D., & Starkman, G. 2007, Phys.Rev., D75, 023507
Copi, C. J., Huterer, D., & Starkman, G. D. 2004, Phys.Rev., D70, 043515
Cruz, M., Martinez-Gonzalez, E., Vielva, P., et al. 2008, arXiv:0804.2904
de Oliveira-Costa, A., Tegmark, M., Zaldarriaga, M., & Hamilton, A. 2004, Phys.Rev., D69, 063516
Draine, B., & Lazarian, A. 1998, Astrophys.J., 508, 157
—. 1999, Astrophys.J., 512, 740
Draine, B. T., & Hensley, B. 2012, ApJ, 757, 103
—. 2013, ApJ, 765, 159
Eriksen, H., Hansen, F., Banday, A., Gorski, K., & Lilje, P. 2004, Astrophys.J., 605, 14
Hansen, F., Banday, A., Gorski, K., Eriksen, H., & Lilje, P. 2009, Astrophys.J., 704, 1448
Hansen, M., Kim, J., Frejsel, A., et al. 2012a, JCAP, 1210, 059
Hansen, M., Zhao, W., Frejsel, A. M., et al. 2012b, MNRAS, 426, 57
Haslam, C., Salter, C., Stoffel, H., & Wilson, W. 1982, Astron.Astrophys.Suppl.Ser., 47, 1
Heiles, C., Chu, Y.-H., Troland, T. H., Reynolds, R. J., & Yegingil, I. 1980, ApJ, 242, 533
Hoftuft, J., Eriksen, H., Banday, A., et al. 2009, Astrophys.J., 699, 985
Kim, J., & Naselsky, P. 2010, Astrophys.J., 714, L265
Land, K., & Magueijo, J. 2005, Phys.Rev.Lett., 95, 071301
—. 2007, Mon.Not.Roy.Astron.Soc., 378, 153
Larson, D., Dunkley, J., Hinshaw, G., et al. 2011, Astrophys.J.Suppl., 192, 16
Mertsch, P., & Sarkar, S. 2013, JCAP, 1306, 041
Naselsky, P. D., Doroshkevich, A., & Verkhodanov, O. 2004, Mon.Not.Roy.Astron.Soc., 349, 695
Naselsky, P. D., & Novikov, D. I. 1995, Astrophys.J., 444, 1
Park, C.-G. 2004, Mon.Not.Roy.Astron.Soc., 349, 313
Roger, R. S., Costain, C. H., Landecker, T. L., & Swerdlyk, C. M. 1999, A&AS, 137, 7
Salter, C. J. 1982, Astrophys.J., 199, 97
Sarkar, S. 1983, Mon.Not.Roy.Astron.Soc., 11, 1
Schwarz, D. J., Starkman, G. D., Huterer, D., & Copi, C. J. 2004, Phys.Rev.Lett., 93, 221301
Wolleben, M. 2007, Astrophys.J., 664, 349